Korean J. Chem. Eng., 33(11), 3134-3140 (2016)
DOI: 10.1007/s11814-016-0182-7

pISSN: 0256-1115
eISSN: 1975-7220

Elemental mercury removal from syngas at high-temperature using activated char pyrolyzed from biomass and lignite

Huawei Zhang*,†, Hongju Shi*, Jiangyan Chen*, Ke Zhao*, Li Wang*, and Yanhong Hao**

*College of Chemical and Environmental Engineering, Shandong University of Science and Technology, Qingdao 266590, P. R. China
**Environmental Engineering College, Shanxi University, Taiyuan 030013, P. R. China
(*Received 25 September 2015 • accepted 28 June 2016*)

Abstract−Activated char obtained by the co-pyrolysis of a mixture of lignite and biomass impregnated with $ZnCl_2$ solution was found to be effective for the high-temperature capture of mercury from syngas. The prepared samples were characterized by X-ray photoelectron spectroscopy, Hg-thermal programmed desorption as well as Brunauer-Emmett-Teller analysis. The results show that activated char exhibits a large surface area as well as abundant micropores and C-Cl, C=O, and COOH functional groups. During the chemisorption of mercury, gaseous Hg^0 is first oxidized by C-Cl to $HgCl_2$; $HgCl_2$ which acts as the intermediate product then reacts with the C=O and COOH functional groups on the surface of activated char to generate Hg-OM. At high adsorption temperatures, Hg-OM on the adsorbent surface can further decompose and generate HgO. The C-Cl group is important for the first oxidation step of gaseous Hg^0, and the formation of $HgCl_2$ is the rate-determining step for the entire process of adsorption.

Keywords: Mercury, Syngas, Activated Char, Adsorption, Desorption

INTRODUCTION

Mercury is a typical heavy metal contaminant that has deleterious effects on the environment and human health. With the growing awareness about the severity of the effects of mercury, there is now global agreement on the need for reducing its emission into the atmosphere. Coal processing and utilization industry is the main contributor to mercury pollution in the atmosphere [1]. Upon combustion and gasification of coal, the mercury in coal is converted into a gaseous form and migrates into the atmosphere, thereby seriously affecting environmental quality. There have been several reports on the different forms of mercury in coal-fired flue gas as well as technologies for controlling mercury emission. Studies on the latter have predominantly focused on the preparation of efficient and inexpensive solid adsorbents, the most popular of which include activated carbon, zeolite molecular sieves, metal oxides, and calcium-based sorbents [2-6].

With the rapid development of large-scale coal gasification technology, several researchers have highlighted the need for the removal and capture of mercury from syngas [7,8]. The technology for the removal of mercury from syngas is quite different from that of mercury from coal-fired flue gas in terms of the adsorption temperature window. The temperature of flue gas before the electrostatic precipitator is generally 100-120 °C, while the temperature of syngas after chilling is 200-350 °C. The adsorbents currently used for the removal of mercury are extremely sensitive to temperature, and the mercury removal performance can be significantly decreased at adsorption temperatures greater than 150 °C [9-12]. Thus, it is imperative to develop new adsorbents that exhibit good thermal stability and high mercury removal efficiency, which can perform at the temperatures required for syngas purification.

The co-pyrolysis of lignite and biomass is a classification transformation process based on the chemical composition and structural characteristics of coal and biomass, and has increasingly been of concern in recent years [13,14]. The char obtained from pyrolysis is an inexpensive adsorption material with a large specific surface area, developed pore structure, and abundant functional groups, and can partly replace activated carbon in the fields of flue gas purification and sewage treatment [15-18]. On the other hand, few studies are available on the capture of gaseous Hg^0 under gasification conditions using the char obtained from the co-pyrolysis of lignite and biomass.

Our previous study showed that lignite char is an ideal material for the adsorption of Hg^0 at low temperatures [19]. In this study, a mixture of lignite and biomass was impregnated with a $ZnCl_2$ solution and pyrolyzed at 600 °C in the N_2 atmosphere to prepare activated char. The surface properties of activated char were characterized in detail, the adsorption characteristics of Hg^0 on the surface of activated char were investigated under simulated temperature conditions for syngas purification (100-360 °C), and the adsorption mechanism was analyzed. In addition, a commercial sulfur loaded activated carbon (ZS-08) was used as benchmark sorbent with mercury removal capability.

MATERIALS AND METHODS

1. Sorbent Preparation

Lignite was sourced from Huolinhe City, Neimenggu Province,

†To whom correspondence should be addressed.
E-mail: sdkdzhw@163.com

China. First, lignite was dried at 110 °C and crushed to a size below 0.3 mm. Second, 20 g of a coal sample was accurately weighed and evenly mixed with 30 g of sawdust (0.4-1 mm). Third, the mixture was impregnated with a 25% $ZnCl_2$ solution and stirred for 12 h at 90 °C, with a solid-to-liquid volume ratio of 1 : 3. Next, the sample was filtered and dried after treatment, followed by pyrolysis in a muffle furnace at 600 °C in a N_2 atmosphere for 1 h. Finally, it was cooled to room temperature and crushed into a powder (80-100 mesh). This sample was named ZnSC. For comparison, the mixture of dried coal and biomass was directly pyrolyzed in a muffle furnace at 600 °C in an N_2 atmosphere for 1 h, followed by cooling and crushing. This sample was named SC. Sulfur loaded activated carbon (ZS-08) was purchased by Zhengsen Chemical Industrial Company, Nanjing, China.

2. Characterization of Samples

The physical properties of the samples were characterized by the Brunauer-Emmett-Teller (BET) method; the surface area and pore size distribution were obtained by adsorption-desorption under N_2 at 77 K using an automatic volumetric multipoint apparatus (SSA-4300). Before measurements, all samples were outgassed at 100 °C for 2 h. X-ray photoelectron spectroscopy (XPS; Thermo ESCALAB 250) was employed with Al Kα radiation ($h\nu$=1486.6 eV) as the excitation source to determine the binding energies of C1s, O1s, and Cl 2p. The C1s line at 284.6 eV was used as reference for the calibration of binding energy.

3. Experimental Methodology and Instrumentation

As shown in Fig. 1, gaseous Hg^0 adsorption experiments were conducted in a fixed-bed reactor equipped with syngas simulation, gas adsorption, and tail gas analysis equipment. An Hg^0 permeation tube (VICI Metronic, Inc. U.S.A.) was used to generate a constant amount of Hg^0 vapor (~50 μg/m^3), which was introduced at the inlet of the gas mixer along with 150 mL/min N_2. The remaining N_2 (850 mL/min) was supplied using a gas cylinder and precisely controlled using mass flow controllers. All the gas components were mixed and preheated to the desired temperature and then passed through a quartz reactor (ID 1.0 cm, length 100 cm). A pipe furnace was employed to keep the quartz tube at the desired temperature during adsorption. The concentration of mercury in the tail gas was measured online with a QM201H mercury analyzer. The limit of detection of QM201H mercury analyzer was 0-100 μg/m^3. The experimental device was used to conduct basic mercury mass balance tests, and the error was less than 5%.

First, adsorbent particles (1.0 g) were mixed with 3.0-4.0 g of inert glass beads at an adsorbent bed height of 1.5 cm. At the beginning of the experiment for the determination of mercury removal activity, the gas stream bypassed the reactor, and the inlet gas was sampled to ensure a stable Hg^0 feed concentration. After stable and consistent mercury feeding was established in the system, Hg^0-containing syngas was added to the reactor and a mercury monitor was used to measure the concentration of mercury in the outlet flue gas.

The mercury removal efficiency (η) of an adsorbent from gaseous Hg^0 can be calculated by formula (1):

$$\eta=(1-C_t/C_0)\times 100\% \quad (1)$$

Here, η is the adsorption efficiency, C_0 is the Hg^0 concentration in the inlet stream, and C_t is the Hg^0 concentration in the outlet stream.

4. Mercury Temperature-programmed Desorption Experiments

Mercury temperature-programmed desorption (Hg-TPD) was employed for studying the state of mercury on the surface of sorbents. In this experiment, 1.0 g of the ZnSC sorbent was treated for 5 h to investigate the adsorption of mercury at temperatures of 100, 260, and 360 °C. The mercury-loaded sorbents were heated from 50 °C to 600 °C at a rate of 10 °C/min under 1 L/min Ar flow. The concentration of the mercury released in the carrier gas was continuously measured by using the QM201H mercury analyzer. Each sample was reduced using a $SnCl_2$ solution before measurement in order to convert to Hg^0 completely.

RESULTS AND DISCUSSION

1. BET

Table 1 lists the specific surface areas and volumes of SC, ZnSC

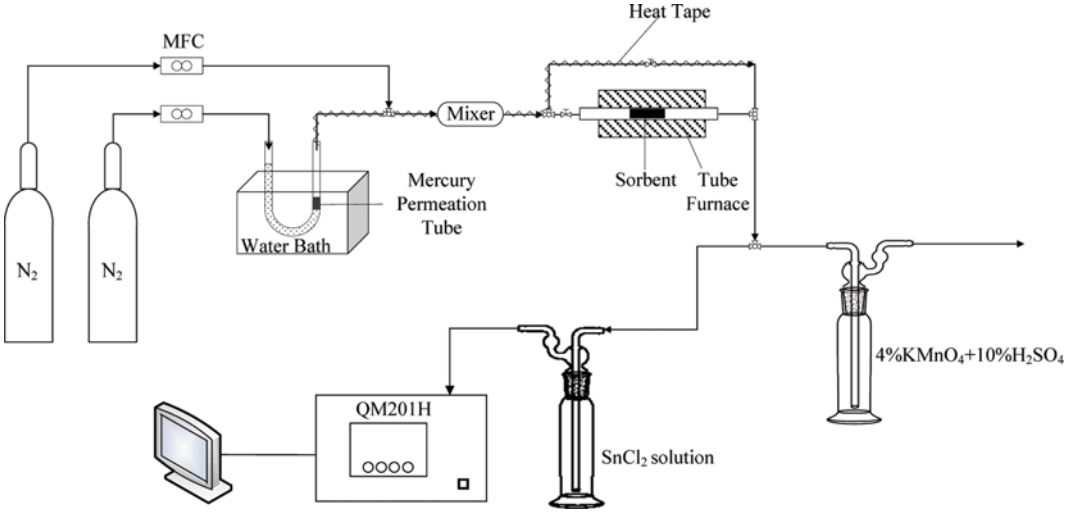

Fig. 1. Experimental device for the adsorption of gas-phase Hg^0.

Table 1. The specific surface areas and volumes of SC, ZnSC and ZS-08

Sample	Specific surface area (m^2/g)	Average pore size (nm)	Total volume capacity (cm^3/g)	Micropore (≤2 nm)		Mesopore (20-50 nm)		Macropore (>2 nm)	
				Volume capacity (cm^3/g)	Proportion (%)	Volume capacity (cm^3/g)	Proportion (%)	Volume capacity (cm^3/g)	Proportion (%)
SC	95.896	6.07	0.0373	0.0232	62.2	0.0125	33.4	0.0016	4.4
ZnSC	1063.948	2.23	0.6644	0.4093	61.6	0.2511	37.8	0.0040	0.6
ZS-08	896.185	4.83	0.4296	0.1667	58.4	0.2509	38.8	0.0120	2.8

and ZS-08. The SC sample exhibited smaller surface area and larger average pore size, and its surface was predominantly composed of micropores and mesopores. Modification by $ZnCl_2$ led to significant increase in the surface area and total pore volume of char. While the specific surface area and total pore volume of SC were 95.896 m^2/g and 0.0373 m^3/g, respectively, the corresponding values for ZnSC were higher at 1063.948 m^2/g and 0.6644 m^3/g, respectively. In addition, the average pore size was reduced from 6.07 nm to 2.23 nm, and the volume of micropores and mesopores increased significantly compared to SC, indicating that ZnSC had a large surface area and a developed porous structure that were superior to those of sulfur loaded activated carbon (ZS-08). This was because the modification by $ZnCl_2$ led to the attachment of the active component $ZnCl_2$ to the surface of biomass and lignite. During pyrolysis, $ZnCl_2$ promoted the dehydration of organic substances and inhibited the production of tar. Additionally, some of the carbon

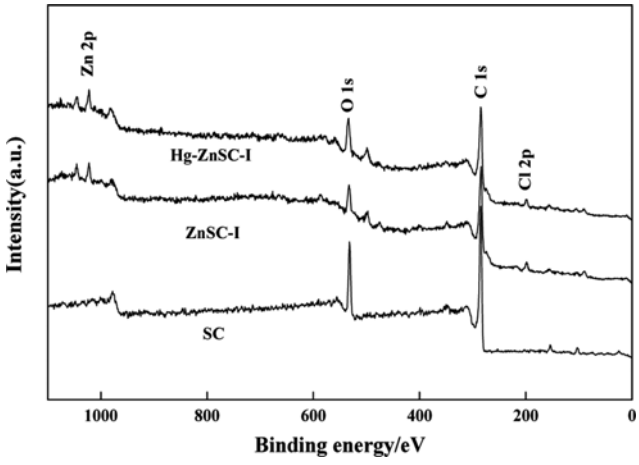

Fig. 2. The XPS spectra of ZSC, ZnSC and Hg-ZnSC.

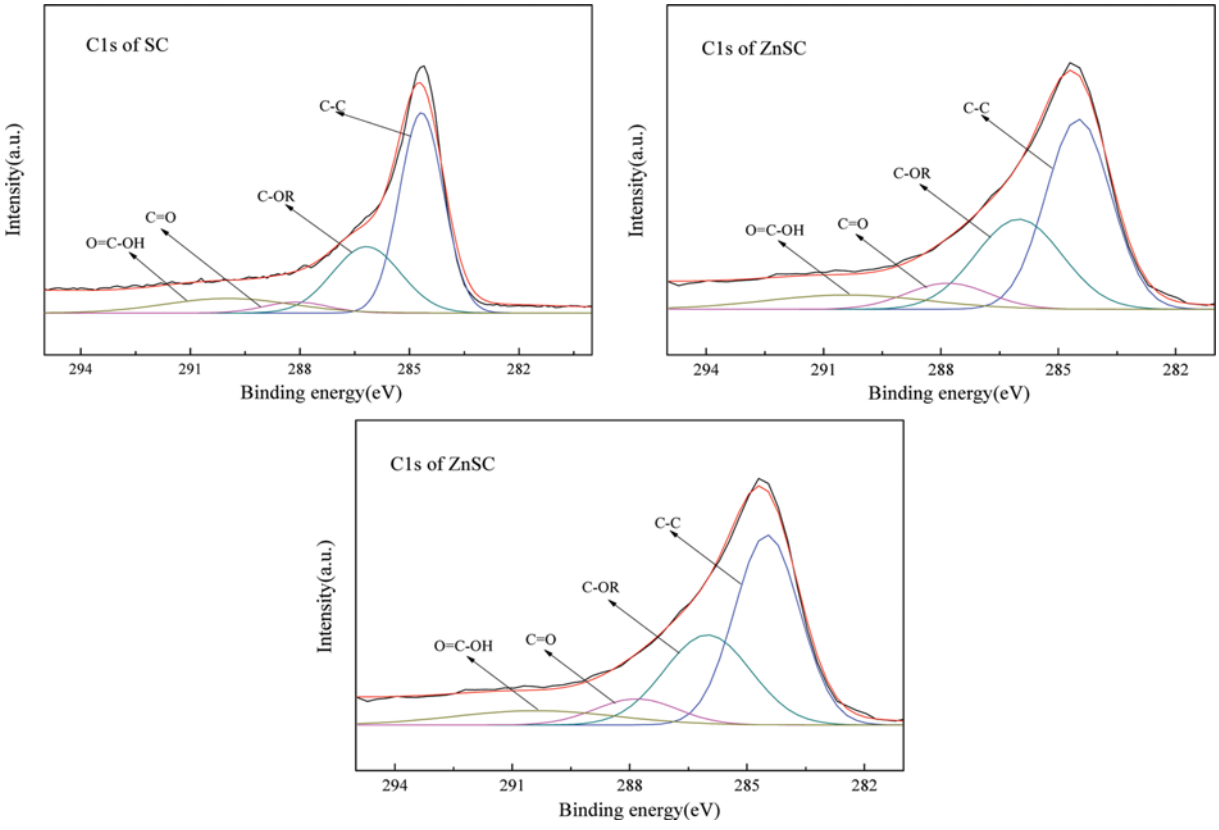

Fig. 3. XPS spectra of C1s for sorbents.

compounds in the biomass and lignite were converted to non-volatile poly-condensation forms, which were deposited on the $ZnCl_2$ molecular framework. Both the dehydration and condensation effects led to the generation of new micropores on the char surface.

2. XPS

Fig. 2 shows the full XPS spectra of SC, ZnSC, and the mercury-loaded sorbent after adsorption at 260 °C (Hg-ZnSC). The main elemental constituents of SC were C and O. After modification by $ZnCl_2$, the Zn 2p peak was centered at 1,023 eV, and the Cl 2p peak was centered at 199 eV, suggesting that either the compound or Zn- and Cl-containing functional groups were formed on the char surface during modification. Since the binding energies of Hg 4f and Si 2p are similar, the Hg 4f energy peak was masked by the Si 2p energy peak from the char, and it was difficult to identify the morphology of Hg^0 adsorbed on the samples by XPS analysis.

For comparing the surface functional groups on the samples before and after $ZnCl_2$ modification as well as mercury adsorption, XPS peak processing software was employed for the simulation of multi-peaks in the binding energy range of C1s and calculation of the elemental ratios among different surface carbon functional groups [20,21]. The results are shown in Fig. 3 and Table 2. The C-C carbon species are the main carbon components on the surface of SC (62.66%), followed by the carbon species C-OR (32.07%), C=O (2.25%), and O=C-OH (3.17%). The amounts of C-O, C=O, and COOH functional groups on the ZnSC surface were higher than those on SC. After the adsorption of mercury, the content of the C-O functional group content on the surface of Hg-ZnSC increased, while the content of C=O and COOH group content clearly decreased. This result suggests that C=O and COOH significantly contribute to the adsorption of gaseous Hg^0, and they can react with mercury to form a mercury complex, Hg-OM [22]. Modification by $ZnCl_2$ led to increase in the C=O and COOH group contents on the char surface, and the modified surface exhibited enhanced adsorption of gaseous Hg^0.

Fig. 4 shows the results obtained from the Cl 2p peak fitting of ZnSC and Hg-ZnSC [23,24]. The Cl element mainly existed in two forms on the activated char surface: covalent C-Cl groups and Cl ions. The main component of ZnSC was covalent C-Cl groups, which accounted for 75.61%. On the other hand, the Cl ion content was only 24.39%. After the adsorption of mercury, the C-Cl group content on the surface of Hg-ZnSC decreased to 24.14%, whereas the Cl ion content increased to 75.86%. This indicates that the C-Cl groups are the active sites for the oxidation of Hg^0. During the adsorption of mercury, gaseous Hg^0 was oxidized to Hg^{2+} by the C-Cl groups which were adsorbed on the micropores of the activated char surface, and most of the C-Cl on the activated char surface was converted to Cl ions.

3. Hg-TPD

The ZnSC samples (1.0 g) containing adsorbed mercury were treated for 5 h at 100, 260, and 360 °C and were subsequently used for TPD experiments. The mass balance of mercury between adsorption and the TPD experiments varied from 95% to 103%. Fig. 5 shows the Hg-TPD results for the Hg-Zn-SC samples. The desorption temperatures of mercury form the surface of three activated chars ranged from 150 °C to 550 °C. For the products of mercury adsorption at different temperatures, the positions of mercury desorption peaks were significantly different, which indicates that the speciation during the adsorption of mercury on the surface of ZnSC is related to the adsorption temperature. The peak fit software was used to fit the overlapping peaks of the TPD curves, and the temperature ranges at which the desorption of mercury compounds occurred were as follows: $HgCl_2$ (210-240 °C), Hg^{2+} combined with oxygen functional groups on the char surface, which corresponds to Hg-OM (270-320 °C), and HgO (350-430 °C) [25-27]. For the mercury-loaded product at 100 °C, the mercury was mainly in the form of Hg-OM, which accounts for 96.03%, with only 3.97% of $HgCl_2$. On the other hand, at the adsorption temperature of 260 °C, the mercury compounds adsorbed on the surface of Hg-ZnSC consisted of 6.37% of $HgCl_2$, 82.43% of Hg-OM, and 11.19% of HgO. At 360 °C, the mercury-loaded product mainly consisted of HgO, which accounts for 79.90%, with only 20.10% of Hg-OM.

Table 2. Functional groups of sorbents from XPS C1s spectra

Functional groups	Electron binding energy (eV)	Relative intensity (%)		
		SC	ZnSC	Hg-ZnSC
C-C	284.5-284.6	62.66	50.32	50.55
C-OR	285.8-286.0	32.07	35.26	43.30
C=O	288.1-288.3	2.25	6.75	3.26
COOH	290.0-290.8	3.17	7.67	2.89

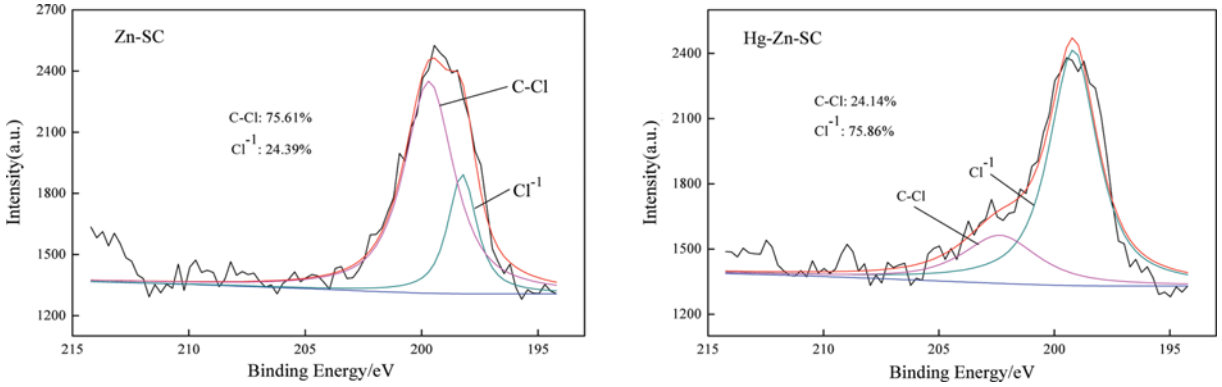

Fig. 4. The XPS spectra of Cl 2p for sorbents.

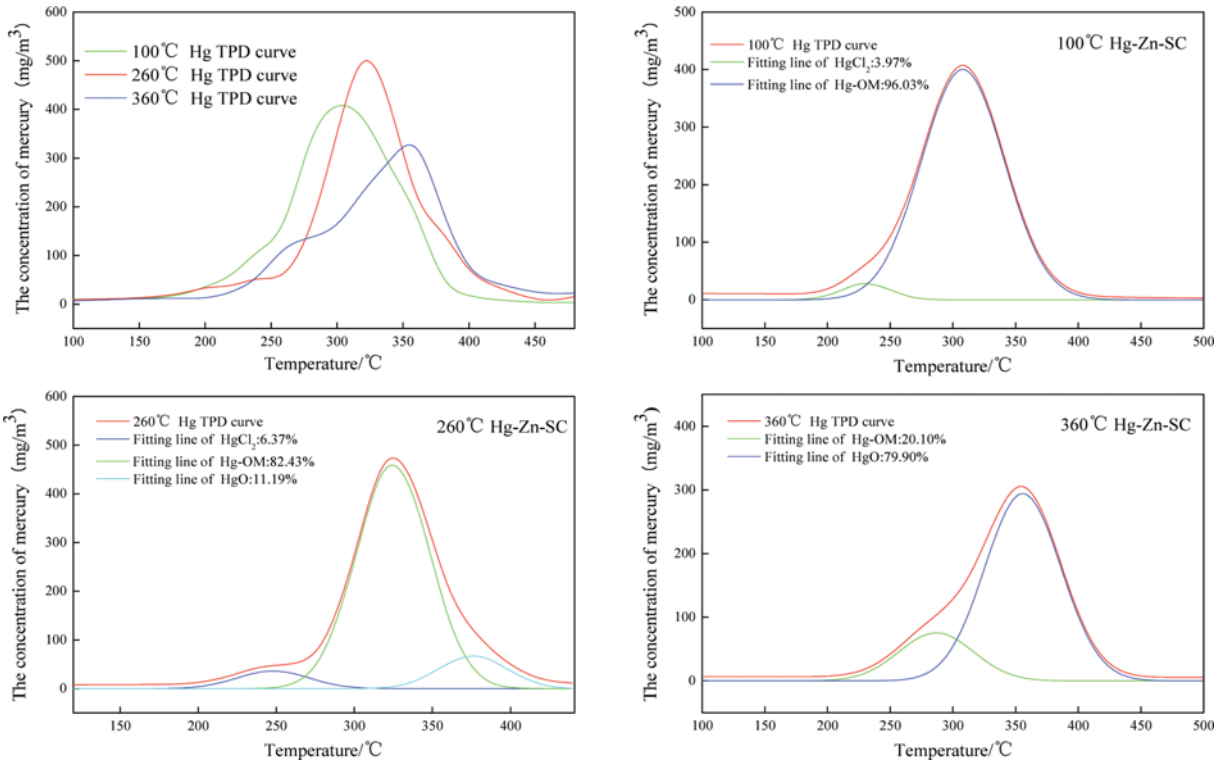

Fig. 5. Hg-TPD spectra of Hg-ZnSC adsorbed at different temperatures.

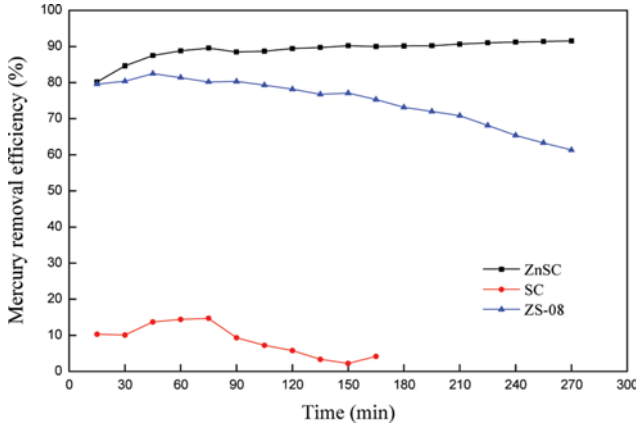

Fig. 6. Mercury removal performance of SC, ZnSC and ZS-08 at 260 °C.

4. Mercury Removal Performance of Sorbents

4-1. Enhanced Effect for the Mercury Removal Efficiency by $ZnCl_2$-modified Activated Char

Fig. 6 shows the mercury removal efficiency of SC, ZnSC and ZS-08 at a mercury inlet concentration of 50 μg/m^3, gas flow rate of 1 L/min, adsorbent dosage of 1.0 g, and adsorption temperature of 260 °C. The mercury removal efficiency of SC was below 20%. Modification by $ZnCl_2$ led to a significant improvement in the mercury removal efficiency, which remained greater than 90% after adsorption for 270 min. The ZS-08 exhibited good removal efficiency during the initial 90 min and decreased sharply thereafter. At higher adsorption temperatures, chemisorption of gaseous Hg^0 mainly occurred on the adsorbent surface, and the mercury removal efficiency was determined by the catalytically active mercury sites, where the oxidation of mercury occurred on the adsorbent surface [28]. Li et al. [23,29-31] reported that C-Cl groups on the surface of carbon-based adsorption materials oxidize gaseous Hg^0 to $HgCl_2$ or other Hg-Cl compounds. Several studies have shown that carbonyl, carboxyl, phenolic hydroxyl, and other oxygen-containing functional groups can effectively promote the oxidation and adsorption of gaseous Hg^0 [32-35]. As observed from the XPS analysis, several C-Cl groups were generated and the amounts of C=O and COOH groups were significantly increased on the surface of ZnSC during modification by $ZnCl_2$. In addition, according to the BET data, the surface area and total pore volume of ZnSC were as high as 1,063.948 m^2/g and 0.6644 m^3/g, respectively, which can effectively adsorb oxidized mercury. Therefore, ZnSC exhibits high mercury removal efficiency.

4-2. Effect of Adsorption Temperature on the Mercury Removal Efficiency of ZnSC

The adsorption temperature significantly affects the mercury removal performance of adsorbents. Fig. 7 shows the mercury removal efficiency of ZnSC at a mercury inlet concentration of 50 μg/m^3, gas flow rate of 1 L/min, adsorbent dosage of 1.0 g, and adsorption temperatures of 100, 260, 300, and 360 °C. When the adsorption temperature increased from 100 °C to 260 °C, the mercury removal efficiency of ZnSC decreased slightly. Further increase in the adsorption temperature beyond 260 °C resulted in a rapid decrease in the mercury removal efficiency, and it decreased to approximately 60% at an adsorption temperature of 360 °C. For the chemisorption of gaseous Hg^0, C-Cl groups on the surface of ZnSC

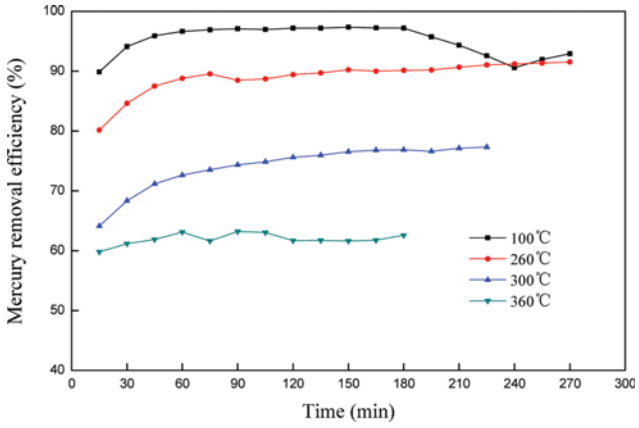

Fig. 7. Effect of adsorption temperature on the mercury removal efficiency of ZnSC.

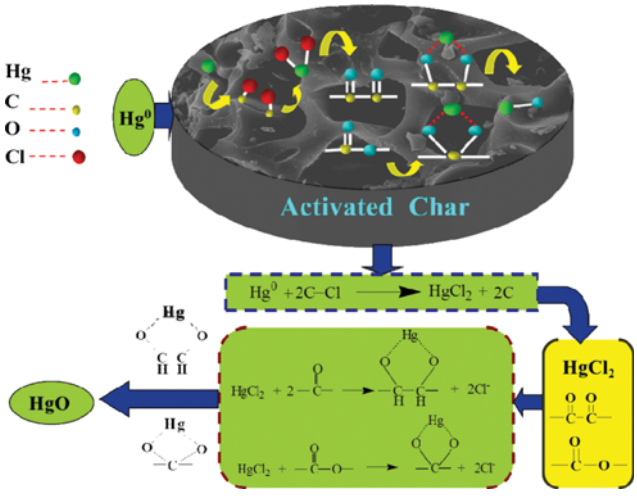

Fig. 8. Mechanism of mercury adsorption.

oxidized Hg^0 to $HgCl_2$. The formation of $HgCl_2$ was exothermic [36], and the increase in the temperature inhibited the forward reaction, thereby decreasing the mercury removal efficiency of ZnSC. Generally, ZnSC exhibited excellent mercury removal performance under high-temperature conditions, and the mercury removal efficiency was maintained at greater than 85% in the temperature range of 100 °C to 260 °C.

5. Mechanism of Mercury Adsorption

The Cl and O-containing functional groups on the surface of ZnSC are the oxidation and adsorption active sites for gaseous Hg^0. The data in Table 1 indicate that ZnSC has a large specific surface area and well-developed pore structure. During adsorption, after the gaseous Hg^0 was spread on the surface, it was physically adsorbed on the micropores on the surface of ZnSC. The physically adsorbed Hg^0 then came into contact with the C-Cl groups and was oxidized to $HgCl_2$. The reaction equations can be described as follows:

$$Hg^0 + ZnSC - surface \rightarrow Hg^0\,(ad) \quad (2)$$

$$Hg^0\,(ad) + C - Cl \rightarrow C - Hg - Cl \quad (3)$$

$$C - Cl + C - Hg - Cl \rightarrow 2C + HgCl_2 \quad (4)$$

From the Cl 2p spectra in Fig. 4, the C-Cl functional group content on the surface of ZnSC was as high as 75.61%, which decreased to 24.14% after the adsorption of mercury. This indicates that a fraction of the C-Cl functional groups on the activated char surface can oxidize gaseous Hg^0 resulting in the generation of $HgCl_2$ during adsorption.

Fig. 5 shows the results obtained from Hg-TPD. The Hg-ZnSC samples with mercury loaded at 100 °C and 260 °C mainly consisted of Hg-OM and a small amount of $HgCl_2$, suggesting that $HgCl_2$ is the intermediate product obtained from adsorption. This product continues to react with the oxygen-containing functional groups on the surface of activated char and generates Hg-OM. At an adsorption temperature of 360 °C, $HgCl_2$ was not detected on the surface of Hg-ZnSC. In addition, the Hg-OM content was low, and the main adsorbed form of mercury was HgO. This shows that most of the Hg-OM on the activated char surface can be decomposed to generate HgO at higher adsorption temperatures. The chemical equation for this reaction can be described as follows:

(5)

(6)

Fig. 8 shows the oxidation and adsorption mechanisms of gaseous Hg^0 on the surface of ZnSC. During the chemisorption of gaseous Hg^0, the C-Cl groups were the important active sites for the first step of Hg^0 oxidation. $HgCl_2$ was the intermediate product, and the reaction resulting in the generation of $HgCl_2$ was the controlling step for the entire process. This step can significantly affect the mercury removal efficiency of the adsorbent. Increase in the adsorption temperature can inhibit the positive reaction, thereby decreasing the mercury removal performance of ZnSC.

CONCLUSIONS

Activated char obtained by the co-pyrolysis of the mixture of lignite and biomass impregnated with a $ZnCl_2$ solution has been prepared as an adsorbent for high-temperature mercury removal. The mercury removal capability of ZnSC is superior to that of SC and commercial sulfur loaded activated carbon (ZS-08). The ZnSC sample exhibits a large surface area and developed pore structure, and its average pore size is in the micropore size range. New C-Cl groups are generated in ZnSC, as compared to SC, and the content of C=O and COOH groups significantly increases. ZnSC exhibits its excellent mercury removal efficiency performance at high temperatures, and the efficiency decreases with the increase in the adsorption temperature. During adsorption, gaseous Hg^0 first diffuses and is physically adsorbed on the micropores of ZnSC. It then contacts with the C-Cl groups and is oxidized to $HgCl_2$, and $HgCl_2$ as the intermediate product reacts with the carbonyl and

carboxyl groups on the surface of activated char to generate Hg-OM. At high adsorption temperatures, Hg-OM on the activated char surface can further decompose to generate HgO. The different forms of mercury on the surface of Hg-ZnSC are related to the adsorption temperature. The C-Cl groups are the important active sites for the first step of Hg^0 oxidation, and the reaction resulting in the generation of $HgCl_2$ is the controlling step for the entire adsorption process. This step influences the mercury removal performance of ZnSC.

ACKNOWLEDGEMENTS

The National Natural Science Foundation of China (51406107 and 21276146) is gratefully acknowledged. The authors would also like to thank the Analytical and Testing Center of Shandong University of Science and Technology, for providing the facilities for the experimental measurements.

REFERENCES

1. E. G. Pacyna, J. M. Pacyna, K. Sundseth, J. Munthe, K. Kindbom, S. Wilson, F. Steenhuisen and P. Maxson, *Atmos. Environ.*, **44**, 2487 (2010).
2. M. A. Lopez-Anton, R. R. Gil, E. Fuente, M. Díaz-Somoano, M. R. Martínez-Tarazona and B. Ruiz, *Fuel*, **142**, 227 (2015).
3. S. Raik, K. Heinz and G. Heinz, *Appl. Catal: B-Environ.*, **144**, 486 (2014).
4. Y. L. Xu, Q. Zhong and X. Y. Liu, *J. Hazard. Mater.*, **283**, 252 (2015).
5. B. K. Zhang, J. Liu, J. Y. Zhang, C. G. Zheng and M. Chang, *Chem. Eng. J.*, **273**, 344 (2014).
6. D. L. Shi, Y. Lu, Z. Tang, F. N. Han, R. Y. Chen and Q. Xu, *Korean J. Chem. Eng.*, **31**, 1405 (2014).
7. S. J. Wu, M. Ozaki, M. D. Azhar and E. Sasaoka, *Fuel*, **87**, 467 (2008).
8. J. S. Zhou, W. H. Hou, P. Qi, X. Gao, Z. Y. Luo and K. F. Cen, *Environ. Sci. Technol.*, **47**, 10056 (2013).
9. H. Zhang, J. Zhao, Y. Fang, J. Huang and W. Yang, *Energ. Fuel*, **26**, 1629 (2012).
10. L. Liu, C. H. Zheng, J. H. Chen, J. S. Zhou, X. Gao, M. J. Ni and K. F. Cen, *Fuel Process. Technol.*, **138**, 15 (2015).
11. Q. Zhou, Y. F. Duan, C. Zhu, J. Zhang, M. She, H. Q. Wei and Y. G. Hong, *Korean J. Chem. Eng.*, **32**, 1405 (2015).
12. F. Scala, C. Anacleria and S. Cimino, *Fuel*, **108**, 13 (2013).
13. X. Yang, C. Y. Yuan, J. Xu and W. J. Zhang, *Bioresour. Technol.*, **17**, 1 (2014).
14. F. Caterina, F. Francesca, O. Alessandro and P. Alberto, *Fuel*, **152**, 138 (2015).
15. C. Z. Wu, M. Song, B. S. Jin, Y. M. Wu and Y. J. Huang, *J. Environ. Sci-China*, **25**, 405 (2013).
16. I. Chowdhury and C. N. Mulligan, *J. Hazard. Mater.*, **190**, 486 (2011).
17. L. J. Leng, X. Z. Yuan, G. M. Zeng, J. G. Shao, X. H. Chen, Z. B. Wu, H. Wang and X. Peng, *Fuel*, **155**, 77 (2015).
18. K. P. Ganesh, C. Shamik and B. Rajasekhar, *Fuel*, **148**, 246 (2015).
19. H. W. Zhang, J. T. Chen, P. Liang and L. Wang, *J. Environ. Sci-China*, **24**, 2083 (2012).
20. J. Shangguan, C. H. Li, M. Q. Miao and Z. Yang, *New Carbon Mater*, **23**, 37 (2008).
21. G. L. Li, B. X. Shen, F. K. Li, L. H. Tian, S. Singh and F. M. Wang, *Fuel Process. Technol.*, **133**, 43 (2015).
22. R. V. Azzi, A. D. Eduardo, I. Dalmázio, D. C. Luis and L. R. Monteiro, *Mater. Res.*, **6**, 129 (2003).
23. G. L. Li, B. X. Shen, Y. Wang, S. J. Yue, Y. Q. Xi, M. D. An and K. K. Ren, *Fuel*, **145**, 189 (2015).
24. J. F. Ma, C. T. Li, L. K. Zhao, J. Zhang, J. K. Song, G. M. Zeng, X. N. Zhang and Y. Xie, *Appl. Surf. Sci.*, **329**, 292 (2015).
25. M. A. Lopez-Anton, R. Perry, P. Abad-Valle, M. Díaz-Somoano, M. R. Martínez-Tarazona and M. M. Maroto-Valer, *Fuel Process. Technol.*, **92**, 707 (2010).
26. B. Zhang, P. Xu, Y. Qiu, Q. Yu, J. J. Ma, H. Wu, G. Q. Luo, M. H. Xu and H. Yao, *Chem. Eng. J.*, **263**, 1 (2015).
27. Z. Q. Tan, J. Xiang, S. Su, H. C. Zeng, C. S. Zhou, L. S. Sun, S. Hu and J. R. Qiu, *J. Hazard. Mater.*, **239-240**, 160 (2012).
28. G. Skodras, I. Diamantopoulou and G. P. Sakellaropoulos, *Desalination*, **210**, 281 (2007).
29. H. L. Li, C. Y. Wu, L. Q. Li, Y. Li, Y. C. Zhao and J. Y. Zhang, *Fuel*, **113**, 726 (2013).
30. S. J. Lee, Y. C. Seo, J. Jurng and G. L. Tai, *Atmos. Environ.*, **38**, 4887 (2004).
31. L. X. Ling, S. P. Zhao, P. D. Han, B. J. Wang, R. G. Zhang and M. H. Fan, *Chem. Eng. J.*, **244**, 364 (2014).
32. L. Tong, W. Q. Xu, H. Qi, X. Zhou, R. H. Liu and T. Y. Zhu, *Acta. Phys.-Chim. Sin*, **31**, 512 (2015).
33. J. Liu, M. A. Cheney, F. Wu and M. Li, *J. Hazard. Mater.*, **186**, 108 (2011).
34. A. Fuente-Cuesta, M. Diaz-Somoano, M. A. Lopez-Anton, M. Cieplik, J. L. Fierro and M. R. Martínez-Tarazona, *J. Environ. Manage.*, **98**, 23 (2012).
35. H. ShamsiJazeyi, *J. Ind. Eng. Chem.*, **16**, 852 (2010).
36. X. C. Lu, J. C. Jiang, K. Sun, J. B. Wang and Y. P. Zhang, *Mar. Pollut. Bull*, **78**, 69 (2014).